Check for updates

Co$_3$O$_4$ nanoparticle modified N, P co-doped carbon paper as sodium carrier to construct stable anodes for Na-metal batteries†

Zhaoqi Liu,[a] Qingwei Zhang,[a] Lin Li [ID][b] and Jinxue Guo [ID] *[a]

Sodium (Na) metal batteries such as Na-ion batteries and Na–CO$_2$ batteries are considered to be excellent alternatives to lithium batteries in terms of their potential applications because of their high specific capacity and low cost. However, the sodium anode showed low efficiency and poor cycling in Na-metal battery performance due to the formation of sodium dendrites and serious corrosion. In this work, nitrogen (N), phosphorus (P) co-doped carbon paper (NP-CP) modified with cobalt tetroxide (Co$_3$O$_4$) nanoparticles was prepared as the Na anode carrier (Co$_3$O$_4$@NP-CP), and a sodium-based composite anode (Na–Co@NP-CP) was further prepared by electrodepositing sodium. The experimental results indicate that the N, P and Co$_3$O$_4$ multi-doped carbon paper has good sodiophilicity, which can induce the uniform plating/stripping of Na$^+$ ions and inhibit the growth of Na dendrites. The N, P doped carbon paper provides a high surface area and tremendous three-dimensional (3D) framework to effectively reduce the areal current density, facilitate the transfer of electrons, and enhance battery life. Therefore, Na–Co@NP-CP based symmetric cells exhibit stable cycling of over 1100 hours at current densities of 1 mA cm^{-2} and fixed capacity of 1 mA h cm^{-2}. When the Na–Co@NP-CP anode couples with CO$_2$, the assembled batteries can deliver a stable cycling of 165 cycles at current densities of 500 mA g^{-1} and limited capacity of 500 mA h g^{-1}. When Na–Co@NP-CP anode couples with Na$_3$V$_2$(PO$_4$)$_3$ (NVP) cathode, the assembled cells exhibit lower hysteresis and batter cycling performance.

Introduction

With the development of society, fossil fuels have been widely used, but they produce huge amounts of greenhouse gases such as carbon dioxide (CO$_2$), which aggravates global warming.[1–3] To address this problem, there is an increasing urgency for the research and development of new energy sources such as Li batteries and Na metal batteries.[4–13] Although lithium (Li) batteries have been developed and widely studied in recent reports, the scarcity of Li in the earth (only 0.002%) limits their application. In contrast, sodium, which accounts for 2.4% of the total elements in the earth, is much more abundant than Li. Consequently, sodium acts as an excellent and cost-effective alternative to lithium in the storage and transformation of energy. Unfortunately, the serious corrosion of the Na anode leads to the poor cycling behaviour in Na metal batteries.

Moreover, the uncontrolled growth of Na dendrites will also lead to the reduction of battery coulombic efficiency, and even lead to battery short circuit, resulting in safety hazards. Therefore, the construction of well-performance anode is the basic premise of the development of Na metal batteries.

To address the issues mentioned above and speed up the development and practical application of Na metal batteries, researchers have proposed a variety of strategies to improve the sodium-based anode. For example, designing electrolyte additives or changing the concentration of electrolyte,[14–16] constructing artificial SEI layers to inhibit the growth of Na dendrites.[17] However, these methods still fail to effectively overcome the volume change of anode and corrosion pulverization phenomenon caused by the uncontrolled growth of Na dendrites or CO$_2$-attacking. Developing three-dimensional (3D) carbon-based or metal current collector as sodium carriers has been confirmed to be an effective way. This approach ensures uniform sodium stripping/deposition, mitigates Na dendritic formation, lowers local current density, and minimizes electrode size variations.[18,19] For example, the Sun and his co-workers have carbonized cotton cloth to form a 3D carbon material with sodiophilicity, and injected molten sodium into the above framework to synthesize the composite anodes, which showed excellent stability and cycling performance.[20] Besides, Dong et al., employed the copper phosphide mesh as the

[a] Key Laboratory of Optic-electric Sensing and Analytical Chemistry for Life Science, MOE, College of Chemistry and Molecular Engineering, Qingdao University of Science & Technology, Qingdao 266042, China. E-mail: guojinxue@qust.edu.cn

[b] Research Center for Green Printing Nanophotonic Materials, School of Materials Science and Engineering, Suzhou University of Science and Technology, Suzhou, 215009, China

current collector for sodium metal electrodeposition, enhancing the battery performances dur to their good sodiophilicity.[21] When compared to chemical polymerization, electrochemical polymerization offers the potential to incorporate a wider range of dopant ions, and also gives better control over film properties, such as thickness and morphology. On the other hand, electrochemical polymerization is comparatively fast, and a major advantage of electrochemical polymerization lies in the fact that the electrical potential may directly be used for polymerization without using any chemical oxidant.[22–24]

Herein, we successfully synthesized Co_3O_4 nanoparticles coated with N and P co-doped carbon paper (Co_3O_4@NP-CP) by electrodeposition, and obtained Na-based Co@NP-CP (Na–Co@NP-CP) anode is further formed by electrodeposited sodium onto the Co_3O_4@NP-CP. The synergistic effect between N, P co-doping and Co base phase not only greatly enhances the sodiophilicity of Co_3O_4@NP-CP framework, but also promotes the highly reversible Na stripping/deposition behavior during the whole cycle, which effectively inhibits the formation of Na dendrites. Moreover, the porous carbon-based skeleton offers sufficient space for sodium storage, effectively enhance the electrical conductivity, and also slowing down the electrode dimension variation. Hence, the Na–Co@NP-CP anode can achieve a stable cycle of more than 1100 h at current densities of 1 mA cm^{-2} in symmetric batteries. Na–CO_2 full battery composed of Na–Co@NP-CP anode can undergo 165 cycles stably at the current density of 500 mA g^{-1} and the limited capacity of 500 mA h g^{-1}. The Na-ion battery, which used NVP as cathode, has shown excellent cycling performance (more than 350 cycles at a current density of 1C).

Experimental section

NP-CP electrode preparation

The anhydrous ethanol and 30% hydrogen peroxide (v/v = 1 : 1) mixed in a 100 mL beaker. After that, the carbon paper with a size of 3 × 4 cm was placed in the above mixture and treated at 60 °C for 24 hours in a drying oven. The treated CP was washed three times with deionized water, and then dried at 60 °C to eliminate residual water. Next, 1.064 g lithium perchlorate ($LiClO_4$) and 2.12 g anhydrous sodium carbonate (Na_2CO_3) are dissolved in 100 mL deionized water to form solution A. Then, 1.04 mL pyrrole and 1 mL phytic acid added in solution A and stirred for 30 minutes to form solution B. In addition, the three-electrode system was constructed with CP (working electrode), platinum wire (opposite electrode) and Ag/AgCl (reference electrode). The above three-electrode system was tested at the voltage of 0.8 V for 15 min in solution B. Finally, the modified CP was pyrolyzed in Ar atmosphere at 800 °C for 2 h to obtain NP-CP.

Na–Co@NP-CP preparation

Firstly, 2.7648 g $Co(NO_3)_2$ dissolves in 100 mL H_2O to form solution C. Then, the three-electrode system was constructed with NP-CP (working electrode), graphite rod (opposite electrode) and Ag/AgCl (reference electrode). The above three-

electrode system was tested at the voltage of −1.0 V for 8 min in solution C to form $Co(OH)_2$@NP-CP. After that, the $Co(OH)_2$@NP-CP was pyrolyzed at 300 °C for 2 h to obtain the Co_3O_4@NP-CP. Finally, we assembled the CR2016 coin battery (the bare sodium as the cathode, Celgard 2400 as the separator, 1 M sodium trifluoromethanesulfonate ($NaCF_3SO_3$, DoDo-Chem) in DIGLYME as the electrolyte) with a current density of 1 mA cm^{-2} and a limited capacity of 20 mA h cm^{-2}. The composite electrode Na–Co@NP-CP was prepared by electrodepositing sodium.

Assembly of the batteries and electrochemical measurements

All batteries were assembled in an Ar-filled glove box with oxygen and water contents <0.01 ppm. The symmetric batteries were constituted with Na–Co@NP-CP or bare sodium (the Celgard 2400 as the separator, 1 M $NaCF_3SO_3$ in DIGLYME as the electrolyte). The Na–CO_2 batteries were assembled by the KB@Ru cathode, the Na–Co@NP-CP or bare sodium anode, the glass fiber membrane (Whatman) separator and the 1.0 M $NaCF_3SO_3$ in DIGLYME electrolyte. The NVP-based full batteries were assembled by the NVP cathode, the Na–Co@NP-CP or bare sodium anode, the glass fiber membrane (Whatman) separator and the 1 M $NaClO_4$ in 1 : 1 v/v vinyl carbonate (EC)/dimethyl carbonate (DMC) with 5.0% fluoroethylene carbonate (FEC) electrolyte. The theoretical capacity of the NVP cathode is 117 mA h g^{-1} and the cathode electrode diameter is 12 mm. It is calculated that the theoretical capacity of the positive terminal of the NVP is 0.3511 mA h cm^{-2}. The theoretical capacity of the negative terminal is 20 mA h cm^{-2}, so the N/P ratio of the whole battery is 56.96. Furthermore, the ESI† given the preparation processes of NVP and KB@Ru cathodes. The electrochemical performance was tested by the LAND battery test system (Wuhan LAND Electronics Co. Ltd).

Results and discussion

Fig. 1a shows the detailed preparation process of Co_3O_4@NP-CP. Firstly, organic materials containing N and P were modified on carbon paper by electrochemical polymerization method using pyrrole and phytic acid as precursors which were further calcinated to form NP-CP. Subsequently, the Co_3O_4@NP-CP were prepared by the electrodeposition craft and following pyrolysis. As shown in Fig. 1b, the scanning electron microscope (SEM) images of NP-CP verify many nanofibers are uniformly coated on the carbon cloth, which is similar to the morphology of its precursor (Fig. S1†), but different from the smooth surface of pure carbon paper (Fig. S2†). As shown in Fig. 1c, many nanoparticles are uniformly covered on the surface of NP-CP, and the obtained morphology of Co_3O_4@NP-CP is significantly different from that of NP-CP (Fig. 1b), indicating that Co_3O_4 has been successfully introduced into Co_3O_4@NP-CP. The transmission electron microscope (TEM) image of Co_3O_4@NP-CP (Fig. 1d) further demonstrates the nanoparticle structure of the Co_3O_4 formed. The high-resolution (HR) TEM image of Co_3O_4@NP-CP shows a planar spacing of 0.46 nm (as shown in Fig. 1d) corresponding to the
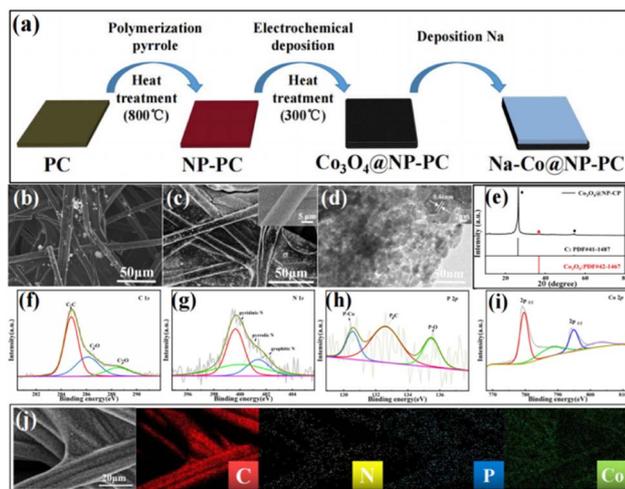
Fig. 1 (a) Schematic diagram for the fabrication process of the Na–Co@NP-CP. SEM images of (b) NP-CP and (c) Co$_3$O$_4$@NP-CP (inset: the corresponding high-resolution SEM images). (d) TEM image (inset: the corresponding enlarged TEM image), (e) XRD patterns of Co$_3$O$_4$@NP-CP and (f–i) XPS spectra of Co$_3$O$_4$@NP-CP. (j) EDX mapping images of Co$_3$O$_4$@NP-CP.
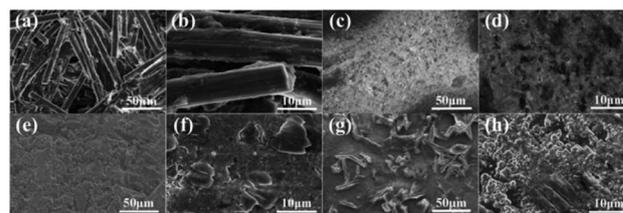

Fig. 2 SEM images of (a and b) Na–Co@NP-CP and (e and f) bare Na electrodes after Na stripping away. SEM images of (c and d) Na–Co@NP-CP and (g and h) bare Na re-plating Na with 20 mA h cm^{-2} at the current density of 1.0 mA cm^{-2}.

(111) crystal surface of Co$_3$O$_4$, further indicating the presence of Co$_3$O$_4$ in the prepared sample. Fig. 1e gives the X-ray diffraction (XRD) pattern of Co$_3$O$_4$@NP-CP and can be seen that a weak band at 37° corresponds to the Co$_3$O$_4$ phase. In order to further study the detailed surface chemical composition of Co$_3$O$_4$@NP-CP, X-ray photoelectron spectroscopy (XPS) has been applied. The surface contents of N, P and Co species were 0.48%, 0.49 and 53.07% respectively, calculated from the full XPS data at Co$_3$O$_4$@NP-CP (Fig. S3†). In the C 1s spectrum (Fig. 1f), the spectra shows binding energies of 284.8 eV (C–C), 286.1 eV (C–O) and 288.5 eV (C=O). The distribution of each N species (Table S1†) are obtained from fitting the N 1s XPS spectra results. In the N 1s spectra (Fig. 1g), two peaks at 399.6 eV, 400.1 eV and 401.3 eV for the Co$_3$O$_4$@NP-CP could be assigned to pyridinic N, pyrrolic N and graphitic N, respectively. The P 2p spectrum of Fig. 1h can identify the P–Co (130.5 eV), P–C (132.6 eV) and P–O (135.4 eV) peaks, while other weak peaks should be pollution peaks. The formation of the Co$_3$O$_4$ phase in Co$_3$O$_4$@NP-CP is further confirmed by high-resolution Co 2p spectrum (Fig. 1i). Fig. 1j is the energy-dispersive X-ray (EDX) mapping technology images of Co$_3$O$_4$@NP-CP, where the elements C, N, P, and Co are uniformly distributed on the fibres. It can be seen that the Na–Co@NP-CP composite anode formed by depositing Na onto the Co$_3$O$_4$@NP-CP matrix has a smooth and flat surface with obvious metallic lustre (Fig. S4†). Na can be well chimeric with Co$_3$O$_4$@NP-CP fibre in Fig. S4,† which proves that Co$_3$O$_4$@NP-CP matrix has splendid sodiophilicity.

In order to research the effect of stripping/plating properties of electrochemical Na on the morphology of sodium anode, SEM images of Na–Co@NP-CP composite anode and bare sodium anode in the symmetric batteries under discharge/charging were displayed at the current density of 1 mA cm^{-2} (Fig. 2). It can be seen from Fig. 2a and b that the Co$_3$O$_4$@NP-CP

fibre skeleton reappear after discharge for 20 h, indicating the stripping process will not damage the structure of Co$_3$O$_4$@NP-CP fibre. In contrast, the surface of bare sodium anode (Fig. 2e and f) becomes bumpy after 20 h of discharge. As shown in Fig. 2c and d, the surface of the Na–Co@NP-CP composite anode is smooth and no sodium dendrites formed after 20 h Na deposition, indicating that Co$_3$O$_4$@NP-CP fibre can integrate well with sodium. The surface of the bare sodium anode (Fig. 2g and h) becomes rough after the same Na deposition, and a large number of sodium dendrites are formed.

To further evaluate the stripping/plating performance of Na–Co@NP-CP composite anode, the bare sodium electrode and Na–Co@NP-CP composite electrode were assembled into symmetrical batteries and then tested at different current densities. As shown in Fig. 3a, the symmetric battery composed of bare sodium electrode has the large and irregular voltage fluctuation at the current density of 1.0 mA cm^{-2} and the limited capacity of 1 mA h cm^{-2}, which suggests the increase of overpotential caused by the formation of sodium dendrites. In contrast, the Na–Co@NP-CP composite anode exhibits stable electrochemical stripping/plating and its overvoltage hysteresis is only 20 mV after 1100 h cycles. The Na–Co@NP-CP composite anode can still maintain the stable discharge/charge curves, when the current density is increased to 3 mA cm^{-2} and the limited capacity is increased to 3 mA h cm^{-2} (Fig. 3b), and its voltages hardly fluctuate after 600 h cycles. Even when the current density is increased to 5 mA cm^{-2} and the limited capacity is 5 mA h cm^{-2} (Fig. 3c), the Na–Co@NP-CP composite anode demonstrates remarkable stability over the cycle of 400 hours. The Na–Co@NP-CP overpotential ranges from 100 to 140 mV at 5 mA cm^{-2} current density, while the initial voltage hysteresis of bare sodium electrode is greater than 400 mV, which fluctuates violently and irregularly during the cycle. Additionally, the rate capabilities of a symmetric cell with a Na–Co@NP-CP composite anode and a bare sodium anode at different current densities (0.5 to 5 mA cm^{-2}) and a capacity of 1 mA h cm^{-2} are compared (Fig. 3d). The voltage polarizations of the Na–Co@NP-CP anode at current densities of 0.5, 1, 2, and 5 mA cm^{-2} are 3, 7, 13, and 35 mV respectively. However, the bare sodium anode exhibits higher voltage polarizations at each of these current densities. These results clearly demonstrate the more excellent cycling stability of the Na–Co@NP-CP anode than bare sodium anode. Fig. 3e and f show the EIS spectra before and after cycling of a symmetric battery composed of Na–
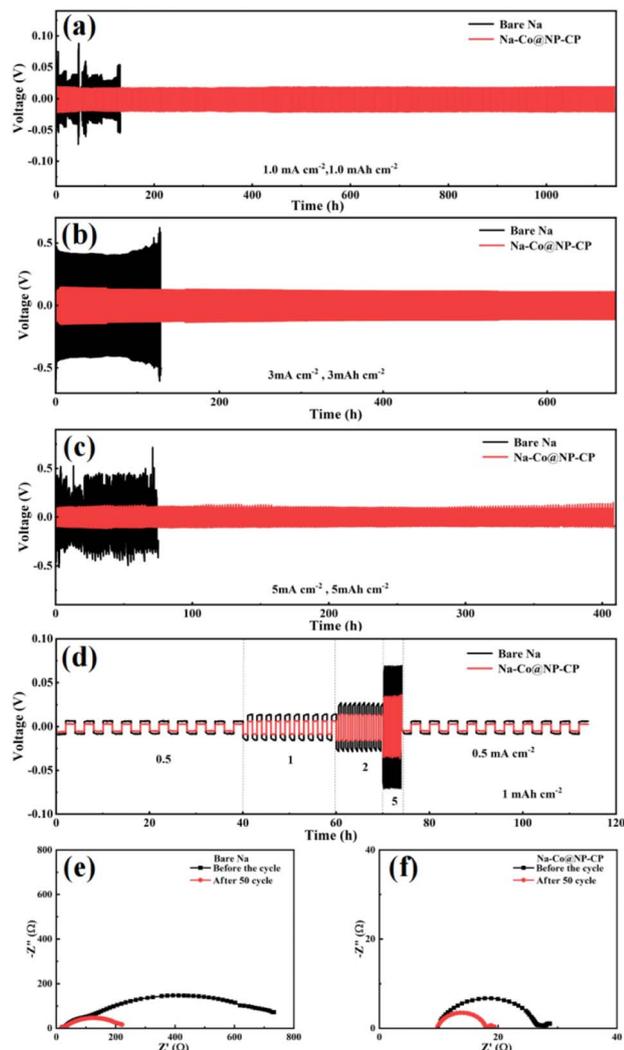
Fig. 3 Galvanostatic discharge/charge profiles of Na–Co@NP-CP and bare Na electrodes in symmetrical cells at various current densities: (a) 1 mA cm^{-2}, (b) 3 mA cm^{-2} and (c) 5 mA cm^{-2}. (d) Rate performance comparison of bare Na and Na–Co@NP-CP of symmetric cells at a current density from 0.5 to 5 mA cm^{-2} with a certain areal capacity of 1 mA h cm^{-2}. Nyquist plots of (e) bare Na and (f) Na–Co@NP-CP based symmetric cells before and after 50 cycles.

Co@NP-CP anode and bare sodium anode at a current density of 1.0 mA cm^{-2} and a fixed capacity of 1.0 mA h cm^{-2}. Generally speaking, the charge transfer resistance (R_{ct}) on the electrode can be reflected by the semi-circle of the high-frequency region in the Nyquist plot.[22,23] As can be seen from Fig. 3e, the interface resistance of the bare sodium electrode is very high before the cycle, which is 732.8 Ω, and the interface resistance drops rapidly to 221.6 Ω after 50 cycles. In contrast, the Na–Co@NP-CP electrode has a very low interface resistance of 28.7 Ω, which slightly drops to 19.3 Ω after 50 cycles. These results indicate that the Na–Co@NP-CP electrode exhibits superior interfacial stability.

To further investigate the performance of Na–Co@NP-CP anode, a Na–CO$_2$ battery was assembled. The Na–Co@NP-CP or bare sodium electrode as anode and KB@Ru as catalytic

cathode (KB@Ru synthesis steps are shown in ESI†). As shown in Fig. 4a and b, the voltage of the bare sodium electrode fluctuates significantly with the increase of the number of cycles, and the overpotential increases rapidly when the current density is 500 mA g^{-1} and the fixed capacity is 500 mA h g^{-1}. And due to the formation of sodium dendrites and the passivation corrosion of bare Na anode, the discharge voltage drops below 1 V after 20 cycle. Surprisingly, although the Na–Co@NP-CP anode also increases in overpotential during cycling, the charge hysteresis increase of this composite anode is slight and its discharge voltage is still about 2 V after 165 cycles. When the current density is increased to 1000 mA g^{-1} and the fixed capacity is 1000 mA h g^{-1} (Fig. 4c and d), the discharge voltage of the bare sodium anode drops below 2 V in the first cycle, and is lower than 1.5 V after 16 cycles. However, the voltage curve of Na–Co@NP-CP electrode shows small fluctuates during the first 60 cycles, although the overpotential also increases, it can still stabilize 125 cycles. As shown in Fig. S5,† the Na–CO$_2$ batteries have a stable cycle performance of more than 100 cycles at the high current density of 1000 mA g^{-1} and the large capacity of
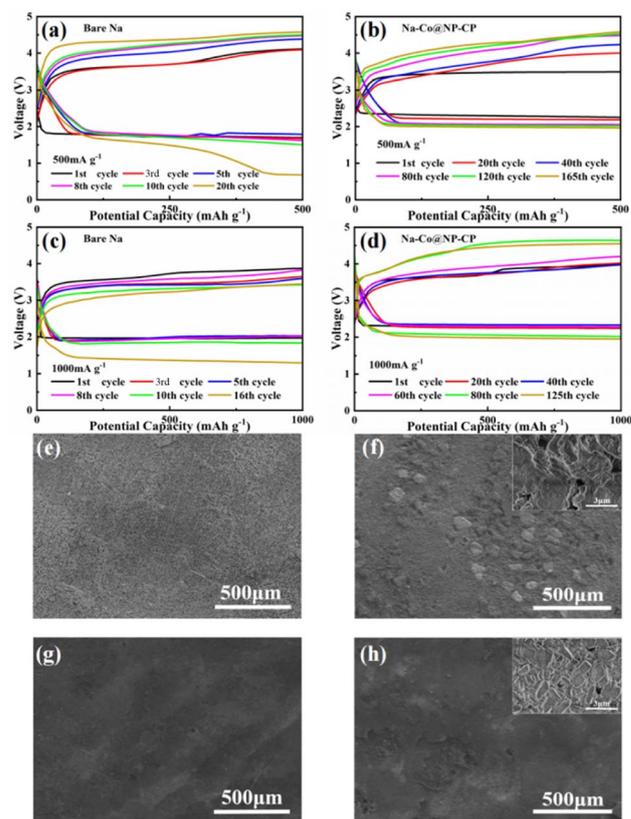

Fig. 4 Voltage curves of the Na–CO$_2$ batteries with (a) bare Na anode and (b) Na–Co@NP-CP anode under the limited capacity of 500 mA h g^{-1} at current densities of 500 mA g^{-1}. Voltage profiles of the Na–CO$_2$ batteries using (c) bare Na anode and (d) Na–Co@NP-CP anode under the limited capacity of 1000 mA h g^{-1} at various current densities of 1000 mA g^{-1}. SEM images of the (e) bare Na, (g) Na–Co@NP-CP anode before cycling, and (f) bare Na, (h) Na–Co@NP-CP anode after 10 cycles in the Na–CO$_2$ batteries under the limited capacity of 500 mA h g^{-1} at the current densities of 500 mA g^{-1}.

1000 mA h g^{-1}. This substantiates the exceptional repeatability of Na–CO$_2$ batteries incorporating Na–Co@NP-CP composite anode. As shown in Table S2,† Na–Co@NP-CP based Na–CO$_2$ battery shows longer cycling life at a high current density and a large capacity compared with several recently reported Na–CO$_2$/air batteries. Fig. 4e–h shows the *ex situ* SEM images of the bare sodium anode and Na–Co@NP-CP anode before and after 10 cycles. It can be seen from Fig. 4e and f that the surface of the bare sodium electrode becomes very rough after 10 cycles, which is caused by the uneven growth of sodium dendrites and sodium corrosion. Conversely, the surface of the Na–Co@NP-CP electrode (Fig. 4g and h) remains notably smooth even after cycling and the crystal morphology can be observed in the enlarged image. These results indicate that Na–Co@NP-CP electrode can inhibit the formation of sodium dendrites and has excellent electrochemical stability.

The bare sodium and Na–Co@NP-CP electrode as anode, NVP as cathode (the preparation of NVP is shown in the ESI†) assembled a complete sodium ion battery to further confirm the excellent performance of Na–Co@NP-CP anode. All the batteries are applied the glass fibre membrane (Whatman) as diaphragm and 1.0 M NaClO$_4$ (dissolving in EC : DMC = 1 : 1 vol% with 5% FEC) as electrolyte. Fig. 5a and b show the discharge/charge curves of the second circle of the Na‖NVP and Na–Co@NP-CP‖NVP batteries. As can be seen from Fig. 5a, Na–Co@NP-CP‖NVP full battery capacity is 125.8 mA h g^{-1} at the initial cycle and Na‖NVP full battery capacity is only 101.1 mA h g^{-1} under 1C (1C = 117 mA g^{-1}). In addition, the overpotential in the second cycle of Na–Co@NP-CP‖NVP battery is also smaller than that of Na‖NVP battery. When the current density is increased

to 5C (Fig. 5b), the capacity of Na–Co@NP-CP‖NVP battery still maintains as high as 89.3 mA h g^{-1}, and the overpotential is also smaller than that of Na‖NVP battery. Fig. 5c and d show the cycling performance of Na‖NVP and Na–Co@NP-CP‖NVP full batteries at the current density of 1C and 5C. In Fig. 5c, the capacity retention of Na‖NVP battery is only 67.1% at 1C, while the Na–Co@NP-CP‖NVP battery is as high as 92.4% over 346 cycles. Even when the current density is increased to 5C (Fig. 5d), the Na–Co@NP-CP‖NVP battery has a capacity retention of 89.6% over 330 cycles and the Na‖NVP battery has a capacity retention of only 75.2%. Fig. 5e shows the rate performance of Na–Co@NP-CP‖NVP and Na‖NVP batteries when the current density ranges from 0.2C to 5C. It can be seen from the Fig. 5e that when the current density increases from 0.2C to 5C, the capacity of the whole Na–Co@NP-CP‖NVP battery decreases from 116.3 mA h g^{-1} at the beginning to 79.5 mA h g^{-1}. When the current density returns to 0.2C, the capacity of Na–Co@NP-CP‖NVP is basically the same as the initial capacity and always higher than Na‖NVP. On the contrary, when the current density of the Na‖NVP battery increases from 0.2C to 5C, the capacity of the Na‖NVP battery rapidly decreases from the initial 97.5 mA h g^{-1} to 48.4 mA h g^{-1}. Fig. 5f shows the cycling curve of Na–Co@NP-CP‖NVP full battery at 1C. It can be seen that its capacity is still above 110 mA h g^{-1} after 346 cycles. Through this comparative analysis, it is evident that the Na–Co@NP-CP‖NVP full battery exhibits a superior battery capacity retention. The Na–Co@NP-CP‖NVP full battery can be stably cycled more than 300 times after multiple tests at 5C current density, which proves that the Na–Co@NP-CP‖NVP full battery has excellent repeatability (Fig. S6†). Furthermore, the excellent stability and cycling properties of the Na–Co@NP-CP composite anode are compared with those reported earlier (Table S3†).

Conclusions

In summary, Co$_3$O$_4$ nanoparticles modified N, P co-doped carbon paper (Co$_3$O$_4$@NP-CP) was synthesized by electrodeposition, and the Na–Co@NP-CP composite anode electrode is subsequently prepared by depositing sodium on Co$_3$O$_4$@NP-CP. The experimental results demonstrate that the incorporation of N, P elements and Co-based substances not only enhances the spatial architecture of the carbon framework and sodium affinity but also induce the uniform plating/stripping of Na$^+$ ions and inhibit the growth of Na dendrites. Therefore, the symmetric battery used Na–Co@NP-CP composite as anode can stabilize the cycle for more than 1100 h at the current density of 1 mA cm^{-2} and the limited capacity of 1 mA h cm^{-2}. When the Na–CO$_2$ full battery used KB@Ru as the catalytic cathode, it can cycle 165 times at the current density of 500 mA g^{-1} and the limited capacity of 500 mA h g^{-1}, and the voltage hysteresis is also smaller than that of the bare Na–CO$_2$ battery. Moreover the Na–Co@NP-CP‖NVP full battery exhibits superior cycling performance, rate performance, and lower overpotential compared to a Na‖NVP battery. This work provides a new strategy for inhibiting the formation of sodium dendrites and developing excellent sodium anode and Na metal batteries.
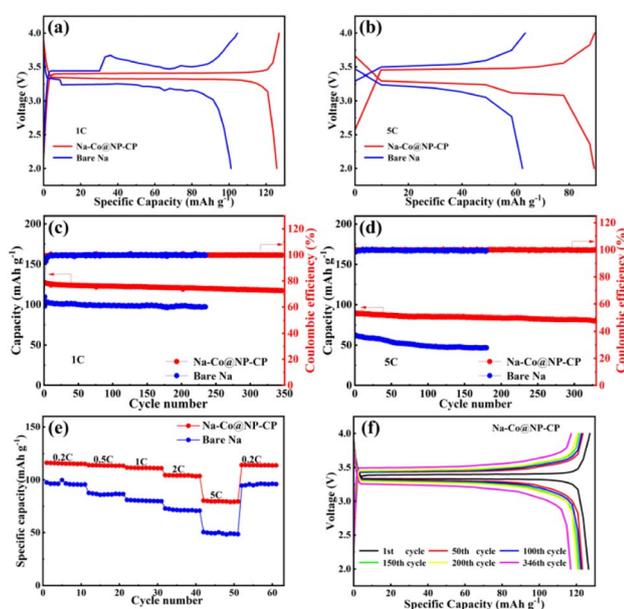

Fig. 5 Galvanostatic charge–discharge curves of Na–Co@NP-CP and Na-based full batteries using NVP electrodes at different current densities: (a) 1C and (b) 5C; cycling performances at (c) 1C and (d) 5C; (e) rate performances of Na–Co@NP-CP or Na-based full cells; (f) Voltage profiles of Na–Co@NP-CP‖NVP at 1C.

Conflicts of interest

There are no conflicts to declare.

Acknowledgements

Notes and references

1 W. Lu, Z. Yuan, Y. Zhao, H. Zhang, H. Zhang and X. Li, *Chem. Soc. Rev.*, 2017, **46**, 2199–2236.

2 J. M. Matter, M. Stute, S. Ó. Snæbjörnsdottir, E. H. Oelkers, S. R. Gislason, E. S. Aradottir, B. Sigfusson, I. Gunnarsson, H. Sigurdardottir, E. Gunnlaugsson, G. Axelsson, H. A. Alfredsson, D. Wolff Boenisch, K. Mesfin, D. F. D. Taya, J. Hall, K. Dideriksen and W. S. Broecker, *Science*, 2016, **352**, 1312.

3 L. Li, S. Peng, J. K. Y. Lee, D. Ji, M. Srinivasan and S. Ramakrishna, *Nano Energy*, 2017, **39**, 111–139.

4 Y. Hou, J. Wang, L. Liu, Y. Liu, S. Chou, D. Shi, H. Liu, Y. Wu, W. Zhang and J. Chen, *Adv. Funct. Mater.*, 2017, **27**, 1700564.

5 H. K. Lim, H. D. Lim, K. Y. Park, D. H. Seo, H. Gwon, J. Hong, W. A. Goddard, H. Kim and K. Kang, *J. Am. Chem. Soc.*, 2013, **135**, 9733–9742.

6 S. K. Das, S. Xu and L. A. Archer, *Electrochem. Commun.*, 2013, **27**, 59–62.

7 K. Takechi, T. Shiga and T. Asaoka, *Chem. Commun.*, 2011, **47**, 3463–3465.

8 J. Li, H. Zhao, H. Qi, X. Sun, X. Song, Z. Guo, A. G. Tamirat, J. Liu, L. Wang and S. Feng, *Adv. Funct. Mater.*, 2019, **29**, 1806863.

9 W. Ma, X. Liu, C. Li, H. Yin, W. Xi, R. Liu, G. He, X. Zhao, J. Luo and Y. Ding, *Adv. Mater.*, 2018, **30**, 1801152.

10 X. Mu, H. Pan, P. He and H. Zhou, *Adv. Mater.*, 2020, **32**, 1903790.

11 J. Xie, X. Wang, J. Lv, Y. Huang, M. Wu, Y. Wang and J. Yao, *Angew. Chem.*, 2018, **57**, 16996–17001.

12 S. Gao, Y. Liu, Z. Xie, Y. Qiu, L. Zhuo, Y. Qin, J. Ren, S. Zhang, G. Hu, J. Luo and X. Liu, *Small Methods*, 2021, **5**, 2001039.

13 X. Hu, J. Sun, Z. Li, Q. Zhao, C. Chen and J. Chen, *Angew. Chem.*, 2016, **55**, 6482–6486.

14 S. Wei, S. Choudhury, J. Xu, P. Nath, Z. Tu and L. A. Archer, *Adv. Mater.*, 2017, **29**, 1605512–1605519.

15 S. Liu, S. Tang, X. Zhang, A. Wang, Q. H. Yang and J. Luo, *Nano Lett.*, 2017, **17**, 5862–5868.

16 E. Im, J. H. Ryu, K. Baek, G. D. Moon and S. J. Kang, *Energy Storage Mater.*, 2021, **37**, 424–432.

17 J. Zheng, S. Chen, W. Zhao, J. Song, M. H. Engelhard and J. Zhang, *ACS Energy Lett.*, 2018, **3**, 315–321.

18 P. Zhang, W. Wang, J. Liu, C. Zhou, J. Zhou, L. Xu and Lu. Chen, *ACS Appl. Nano Mater.*, 2021, **4**, 3619–3630.

19 S. Ni, S. Tan, Q. An and L. Mai, *J. Energy Chem.*, 2020, **44**, 73–89.

20 H. Liu, M. Osenberg, L. Ni, A. Hilger, L. Chen, D. Zhou, K. Dong, T. Arlt, X. Yao, X. Wang, I. Manke and F. Sun, *J. Energy Chem.*, 2021, **61**, 61–70.

21 P. Xu, X. Li, M. Yan, H. Ni, H. Huang, X. Lin, X. Liu, J. Fan, M. Zheng, R. Yuan and Q. Dong, *J. Mater. Chem. A*, 2021, **9**, 22892.

22 A. Shukla, D. Das and K. Sen, *J. Appl. Polym. Sci.*, 2023, **140**, e53443.

23 J. Rajendran, *J. Hazard. Mater.*, 2023, **449**, 130979.

24 J. Rajendran, A. N. Reshetilovb and A. K. Sundramoorthy, *Mater. Adv.*, 2021, **2**, 3336.